Automatization of the Interferometric Process for Visualization and Management of Spatial Data

Steven Edward Coelho dos Santos
steven.santos@tecnico.ulisboa.pt

Instituto Superior Técnico, Lisboa

January 2021

Abstract

In last years, the number of sensors that capture images of land surface has increasing, as a result of a strong bet of many countries and space agencies. Due to that, large amount of data has been recorded and their integration in a single viewer platform is of utmost importance to support informed decisions.

Images captured by Synthetic Aperture Radars (SAR) sensors have been selected in this study, as they are acquired by active sensors and more independent of meteorological conditions. Among of the various sensors that operate in radars' wavelength, the Sentinel-1 mission, part of the Copernicus program, was used as the base to the development of this thesis.

The phase difference between two images obtained with different acquisition geometries, for the same scatter target, allows the determination of object's altitude, based on interferometric technique and its application to SAR images it is known as Interferometric Synthetic Aperture Radar (InSAR) technique, capable of measure displacements in the scale of millimeters with high special and temporal resolutions. This phase difference contains several contributions such as the topography and the atmosphere effect, which acts as perturbation factor, especially, when the goal is to compare interferometric products.

The main objective of this study was the automatization of the interferometric process, starting with the download of SAR images until their visualization in a WEBGIS platform. To reach this, a set of scripts, capable of perform the necessary tasks, was created.

Keywords: SAR Interferometry, Synthetic Aperture Radar, Sentinel-1, SNAP, GACOS, Spatial data infrastructure.

1. Introduction

Synthetic Aperture Radars (SAR) sensors acquires images in the microwave spectrum, useful in many applications. They are active systems that give them the ability to function independently of sunlight and in more adverse weather conditions.

SAR images are complex since each pixel simultaneously records the amplitude and the phase: the amplitude provides information about the characteristics of the target and the phase records information concerning the distance between the sensor and the object to be mapped.

The estimation of the phase difference from two images obtained with different acquisition geometries, for the same retro-dispersor element, allows the determination of the object's altitude, in a technique called interferometry and its use based on SAR images is known as Interferometric Synthetic Aperture Radar (InSAR). These techniques are capable of measuring changes in the millimeter scale with high spatial and temporal resolution, thus proving to be very promising.

The Copernicus program, an Earth observation program led by the European Commission in partnership with the European Space Agency (ESA), led to the launch of the Sentinel-1 (A/B) mission in 2014, which allowed a systematic global mapping of the Earth's surface by SAR images.

It should be noted that, similar to Copernicus, there are other programs from different space agencies, with similar facilities, such as the *Deutsches Zentrum für Luft- und Raumfahrt* (DLR) which provides TerraSAR-X images; *Agenzia Spaziale Italiana* (ASI), which makes COSMO-SkyMED images available; Japan Aerospace Exploration Agency (JAXA) which makes ALOS–Palsar images available and the Canadian Space Agency (CSA), which makes RADARSAT images available [2, 6, 13, 26].

2. Theoretical Background

2.1. SAR images

The images acquired by SAR sensors are complex images. The echo recorded is constituted by an amplitude and phase value of the signal, resulting in a complex matrix in which each pixel has a value with a real and imaginary component. The amplitude is responsible for providing information regarding the characteristics of the object's surface and the phase registers information regarding the distance between the sensor and the

ground/object [3].

These systems illuminate the Earth's surface with lateral geometry (Side Looking Airborne Radar - SLAR), where they transmit microwave pulses according to the plane perpendicular to the trajectory, called the Ground Range. The direction of movement of the platform is known as Azimuth direction and is obtained from signal processing. The measured distance between the radar and the object is called the Slant-Range.

The range of variation of the most common wavelengths in SAR systems is between 0.75 cm and 120 cm, distributed in seven spectral bands Ka, Ku, X, C, S, L, and P, being L, C and X the most used bands. [16, 31].

2.2. Sentinel 1

There is currently a diversity of missions that allows the global mapping of the earth's surface. For the present work, images from Sentinel 1 were used as a data/information source, since Portugal is an ESA member country, which provides the availability of images almost in real time and without costs.

Sentinel-1 consists of a constellation of two satellites, Sentinel-1A and Sentinel-1B, 180 degrees apart, incorporates a SAR instrument that operates in the C band with four image acquisition modes, with different resolutions (5 m) and coverage (400 km) [14]. This mission offers double polarization capabilities, very short revisit times and product availability. The two satellites together provide at least two measurements from the European continent every six days and from almost all the territory outside Europe, with regular intervals of 6, 12 or 24 days [15]. The four image capture or acquisition modes, Strip Map (SM), Interferometric Wide Swath (IW), Extra Wide Swath (EW) and Wave (WV), produce or make available SAR products at three levels: level 0, level 1 and level 2 [15].

2.3. SAR interferometry

Radar interferometry explores the images acquired with synthetic aperture radars, observing the same area with slightly different angles. This acquisition can be made simultaneously, with two radars on the same platform, called single-pass interferometry, or at different times, called repeat pass interferometry [18, 28].

The phase of the SAR image is mainly determined by the distance between the satellite antenna and the ground targets. The SAR interferogram is generated by the multiplication, pixel by pixel, of the first SAR image with the complex conjugate of the second [18]. The amplitude of the interferogram is the amplitude of the first image multiplied by the second, while the interferometric phase is the phase difference between the images.

This phase difference results in a new "image", called interferogram, a fringe pattern that contains all the information related to the geometry of the terrain, target or object. The interferogram phase is highly correlated with the topography of the terrain. In this way, the difference in interferometric phase ($\Delta\phi$) is proportional to the displacement (ΔR) divided by the transmitted wavelength (λ), according to:

$$\Delta\phi = \phi_1 - \phi_2 = \frac{4\pi}{\lambda}\Delta R\,. \tag{1}$$

In the phase difference there are several contributing factors, such as the flat Earth phase, the topographic phase, atmospheric conditions (humidity, temperature and pressure change between the two acquisitions), and other noises and, finally, the eventual superficial deformation that occurs between the two acquisitions [18, 37].

The relationship between the height of a point on the reference surface and the absolute phase difference obtained from a pair of SAR images given by:

$$\delta H = \frac{\lambda R sin(\theta_0)}{4\pi B cos(\theta_0 - \alpha)}\delta\phi\,. \tag{2}$$

θ_0 is the elevation angle of one satellite in relation to the reference surface, α the angle of inclination between the sensors, R the distances from the same satellite to the object/target on the Earth's surface and B the interferometric baseline [18, 23].

2.4. Steps of the interferometric process

The different acquisition geometries together with the fact that the navigation directions of the sensors are not exactly parallel, determine that the acquisition grids are not coincident, with variation in scale, rotation and translation. Thus, it is necessary a sequential procedure that begins with the registration of images, construction of the interferogram, determination of coherence, filtering and resampling.

2.4.1 Registration

The first operation consists of registering the images, where one is chosen to be the master and the other images are the slaves. The pixels in the slaves images will be moved to align with the master image. The register ensures that each terrestrial target contributes to the same pixel (range, azimuth) in both the master and slave images.

The registration is carried out in general in two stages. The first phase is called coarse registration and consists of registering one image over the other with resolution of an image element. The second phase, in turn, called fine registration, consists of registering one image over the other with resolution of the sub-image element, involving resampling.

2.4.2 Interferogram Formation

After the image registration process is completed, the interferogram is generated from the cross multiplication from element to element of the master image with the complex conjugate of the slave [18].

2.4.3 Determination of Coherence

Coherence is a measure that allows to measure the level of correlation between two images, ranging from zero (no correlation) to 1 (maximum correlation). When applied to an interferometric pair it is an indicator of quality. In this way, the coherence analysis allows the selection of image pairs for exploration in interferometric

applications. This is useful information when analyzed within a certain time or space [40].

2.4.4 Filtering

After the formation of the interferogram, the phase difference can be corrupted by temporal and geometric de-correlation noise, volume dispersion and other processing errors. The phase information in de-correlated areas is not restored, however the quality of the existing fringes in the interferogram can be increased by applying specialized phase filters, such as the Goldstein filter that uses a Fast Fourier Transform (FFT) to increase the signal ratio image noise [21].

2.4.5 Multilooking

Multilooking processing represents a spatial average of the complex components of the signal and is applied over complex interferograms from an average window determined to reduce the statistical variation of noise. In other words, it is used as an efficient algorithm to reduce noise phase in an interferometric image [25]. Multilooking can improve the reliability of the phase unwrapping, while reducing spatial resolution [22].

2.4.6 Phase unwrapping

In order to be able to relate the interferometric phase to the topographic height, firstly the phase must be unwrapped. Phase ambiguity is defined as the difference that generates a continuous interferometric phase change of 2π in the curled interferogram.

According to Zebker et al. [45], the performance of the phase unwrapping algorithm depends on two factors: the signal to noise ratio (SNR) of the interferogram and the spacing between the interferometric fringes. The two main approaches to phase unfolding are local and global methods. Local methods include algorithms based on residues, as proposed by Goldstein et al. [22], and growing regions. The objective is to identify and isolate the points where there is a phase inconsistency, in order to avoid the propagation of error during the unwinding. The global methods seek to minimize the global error through, for example, the least squares method proposed by Zebker and Lu [44] and multi-resolution techniques, among others.

2.5. Spatial data platforms

The constant advances in spatial data infrastructure (IDE) and responsible entities, along with the growing volume of data produced daily, allows us to say that it is necessary to give importance not only to technical and infrastructure issues, but also to issues of accessibility of the data involved by these structures. With the technological advances of the internet and its associates, excellent conditions have been created for the development of favorable environments for the publication, access, exploration and distribution of information and geographic data.

2.5.1 Spatial Data Infrastructures

The concept of spatial data infrastructures (IDE), which was originated in the early 1990s [12], encompasses a technological, political structure, with the standards and human resources necessary to acquire, process, store, disseminate and use geographic information effectively. These infrastructures, through resource sharing, avoid redundant efforts and reduce the cost of producing new databases or existing databases [5, 34, 35].

IDEs can exist at different levels of intervention in the territory, from the corporate and local level (smaller areas but with greater levels of detail), up to regional and global levels [36].

A fully functional IDE architecture should provide users with the possibility and functionality to discover the type of data they are looking for, to view it and access it online. In this way, Geoportals can be seen as components of these infrastructures [29, 39].

Like any infrastructure, an IDE implies the existence of some kind of coordination for the formulation and implementation of policies, in addition to the production of metadata with certain standards [29].Formal policy and the legislative environment within which the IDE initiative is found is an important consideration, and alignment with policy priorities is critical to its success.

IDEs are composed of a set of technical and non-technical components that facilitate the sharing of geographic information: data, metadata, network services and sharing agreements [10].

Conceptually, the IDE architecture consists of data, service providers and consumers who use applications to access spatial information [19]. The implementation of these infrastructures has been carried out using Service-Oriented Architectures (SOA), thus allowing to be independent of technologies [4].

They follow several standards or norms defined by the Open Geospatial Consortium (OGC), such as the Web Feature Service (WFS) and the Web Map Service (WMS) [27].

2.5.2 Examples of spatial data platforms

InSAR Norway

InSAR Norway is a free and open mapping service for the entire Norway of InSAR data. It started in 2016 as a joint partnership between Geological Survey of Norway (NGU), Norwegian Water Resources and Energy Directorate (NVE) and Norwegian Space Center, with the aim of establishing or implementing a national land movement center [33].

It is a service based on a Persistent Scatterer (PS) flow (technique that focuses on identifying pixels in SAR images, characterized by low noise values [24]) for Sentinel-1 data, updated every 12 months.

Production is performed in a dedicated cluster consisting of 19 high-performance processing nodes with the following characteristics:

- 14 physical Central Processing Unit (CPU);
- 512 GB Random Access Memory (RAM);
- Fast access to large storage system (2 PB).

The production cycle currently runs once a year with a total duration of 80 min per processing unit per vCPU [11].

National Geoportal

Geoportale Nazionale (GN), is an Italian geoportal, managed and maintained by the Ministry of Environment and Protection of Land and Sea. It is a management and sharing system for territorial and environmental data, based on webGIS technologies.

The platform allows or makes available a map viewer, a metadata catalog that allows data search and a set of services according to the standards of the Open Geospatial Consortium (OGC), which allow the visualization, data download and processing data (using WMS, WFS and WCS services) [32, 38].

3. Materials and Methods

3.1. Download SAR products

The SAR images, from the Sentinel-1 mission, provided by ESA's platform for the Copernicus Program, will be used. For ESA member countries, the use of SAR images is generally free.

As one of the main objectives is the automation of processes, the development or use of tools that speed up the acquisition of images was made without having to manually resort to the platform, which are APIs and Batch Scripting. The built solution uses the *dhusget* script [17] that allows the parameterized configuration of the product download. Since the script can only be used in a LINUX environment, a Python script, *download.py*, was developed, which, through a configuration file, *download.conf*, pre-filled with the desired parameters, performs the search and ensures it the respective download of the products. For this script, a library named Sentinelsat was used, which facilitates the search, download and retrieval of Sentinel image metadata [1].

3.2. Processing of SAR images

From the diversity of existing software for interferometric processing, the SNAP (Sentinel Application Platform) software supplied by ESA was chosen due to its free and open access, its configuration to use the images available under the Copernicus Program and for allowing the data processing from the command line.

In order to automate the processing of images, Python and Matlab programming languages were used and scripts were developed, capable of performing tasks that previously had to be done manually. Thus, the image processing was divided into eight stages or processes (figure 1).

Automation started with the construction and later organization of: scripts, SLC products obtained previously, xml graphics, topographic delay maps in separate directories, creation of configuration files and directories for which results, process logs are saved. Furthermore the executable (SNAPHU - Statistical-Cost, Network-Flow Algorithm for Phase Unwrapping [7–9]) which is responsible for the phase unwrapping of the interferograms.

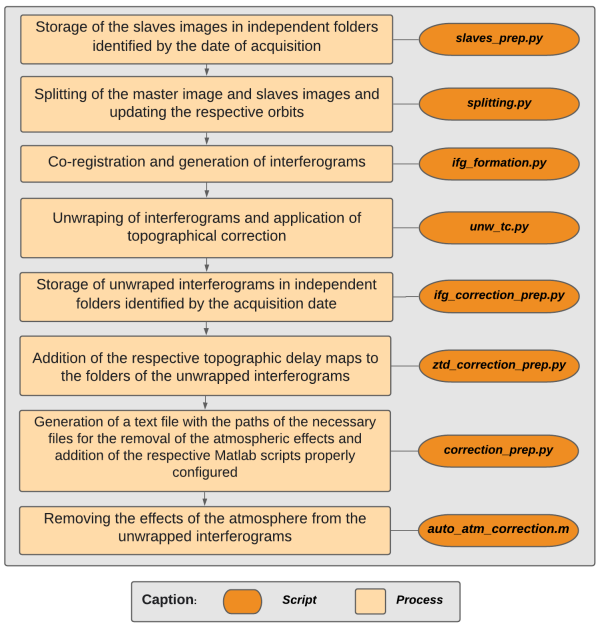

Figure 1: Image processing steps.

3.2.1 Interferometric processing

The SNAP architecture provides a Graph Processing Framework (GPF) that allows the user to create graphs in XML format, in order to allow mass processing and custom processing chains and to do the processing from the command line.

In the logic of process optimization, it was decided to divide the process (figure 2), in three stages (figure 3) resulting in four main graphics (nine in total): *split_applyorbit.xml*, *coreg_ifg_ml_flt.xml*, *snaphuexport.xml* and *snaphuimport_tc.xml* (figure 4). Each process is equivalent to a graph with the exception of the third and last process, which is separated into two.

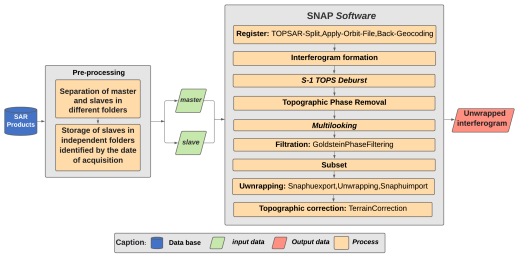

Figure 2: Flowchart of interferometric processing.

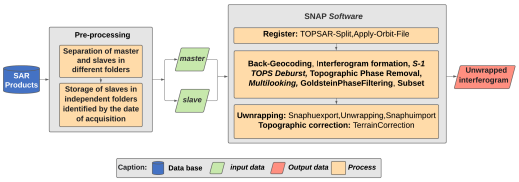

Figure 3: Flowchart of condensed interferometric processing.

(a) split_applyorbit

(b) assemble_split_applyorbit

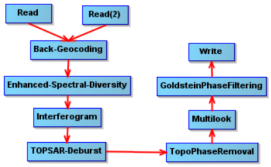

(c) coreg_ifg_ml_flt

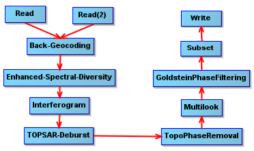

(d) coreg_ifg_ml_flt_subset

(e) snaphuexport

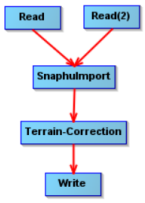

(f) snaphuimport_tc

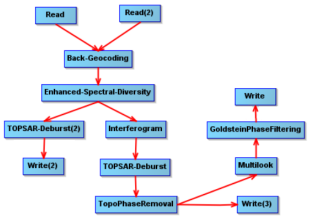

(g) coreg_ifg_ml_flt_export

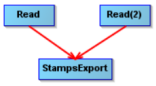

(h) stampsexport

Figure 4: XML graphics responsible for the interferometric process.

The first process, through the *split_applyorbit.xml* graph, is responsible for splitting the master and slave(s) and updating the respective orbits. If the slaves cover only part of the master's area of interest, it is possible to use the corresponding slices to ensure complete coverage of the area with the assembly of the slaves. In this case, the graph *assemble_split_applyorbit.xml* is used.

The second process, using the *coreg_ifg_ml_flt.xml* or *coreg_ifg_ml_flt_subset.xml* chart (if necessary a subset), forms and makes the interferograms available. If it is necessary to export to STAMPS (Stanford Method for Persistent Scatterers) [30], the script, by setting the appropriate parameter in the configuration file, is able to select another graph (coreg_ifg_ml_flt_export.xml or coreg_ifg_ml_flt_subset_export.xml, if necessary a subset), which, in addition to providing the interferograms mentioned above, provides the co-registrations of SLC products and interferograms. The export is done with the aid of the *stampsexport.xml* chart.

The third and last process is divided into three parts and uses two xml graphics, *snaphuexport.xml* and *snaphuimport_tc.xml*. The *snaphuexport.xml* graph is responsible for exporting in order to be able to unwrap it with SNAPHU, while the *snaphuimport_tc.xml* graph is responsible for importing the unwrapped data and applying topographic correction. This division was due to the impossibility of unwrapping with the aid of the GPF. The executable *snaphu* was downloaded, which with the help of the *unw_tc.py* script, executes the unwrapping of the interferograms in a chain.

3.2.2 Atmospheric correction

One of the factors most contributing to the phase of the interferogram are the atmospheric conditions. This effect is especially disturbing when the aim is to compare interferograms. To mitigate this effect, an online atmospheric correction service was used, called Generic Atmospheric Correction Online Service for InSAR (GACOS - http://www.gacos.net/), which using an Iterative Tropospheric Decomposition (ITD) model, generates maps, in a binary format, of zenith high delay with high spatial resolution to correct InSAR measurements [20, 41–43].

The tropospheric correction is applied to the interferograms, subtracting or adding the delays from the differentiated atmosphere (difference between the delay maps for the two dates), depending on the choice of the master and slave images in the generation of the interferograms (figure 5).

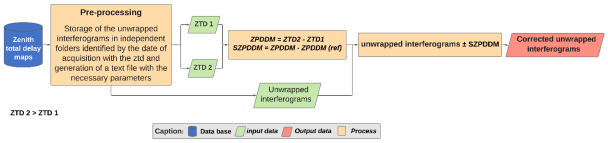

Figure 5: Flowchart of atmosphere correction processing.

GAGOS apart from to providing tropospheric delay maps, it also presents a MATLAB software toolbox, *GACOS_Utility*, which applies the correction. Some pre-processing is necessary in order to have the interferogram data available for this processing. In this way, a script was developed, *atm_correction.m*, capable of reading the data from an interferogram and then applying the correction. In addition to *atm_correction.m*, another script was created, *main_auto_atm_correction.m* which, through a text file, *atm_correction.txt*, generated during pre-processing, with the necessary parameter and parameter paths, allows perform chain processing.

3.3. Comparison between corrected interferograms

The script *main_auto_atm_correction.m* using the function *check_diference.m* that was developed, makes a percentage comparison, calculates the Structural Similarity Index (SSIM) and the Means Squared Error (MSE) between the interferogram being processed and the processed in the previous instant. These are crude comparisons that allow us to perceive the behavior over time of the processed interferograms. The percentage comparison is made at the pixel level. Therefore, a subtraction

is made between the corrected interferograms where the number of different pixels is counted, which is later divided by the total number of pixels. Structural similarity is calculated using the Matlab function *ssim*, which is based on the calculation of three terms: luminance, contrast and structure [46]. The mean square error is calculated using the Matlab *immse* function.

The data is calculated and written in a text file called *ifg_comparation.txt* during atmospheric correction.

3.4. Visualization of spatial data

In order to view the interferograms after removing the effect from the atmosphere, all process data and an image with the interferograms before and after the correction are saved. Corrected interferograms are also exported to GeoTIF during processing. Therefore, to view the data, you only need an application capable of reading the files mentioned above, and this application or platform can be built on the basis of a list of previously identified requirements or an existing one.

4. Case study

The area under study corresponds to the municipalities of Lisbon, Oeiras and Cascais, belonging to the Metropolitan Area of Lisbon, with a total dimension of 243 km^2. The time period considered for the study is between July 2019 and June 2020. Only data from one of the Sentinel-1 satellites and a single direction of acquisition of this information were considered.

4.1. SAR Image Processing

4.1.1 System requirements

The generation of interferograms is a process that consumes a lot of computational resources, so it is recommended at least a quad-core CPU with 16 GB of RAM. In order to be able to process the equivalent of one year of spatial data while maintaining the same master, approximately 140 GB of free disk storage space would be required.

4.1.2 SAR images

In the table 1, we can find the main or necessary characteristics related to SAR images, in order to be able to carry out the processing taking into account the area of interest.

Sensor	Acquisition mode	Direction	Level	Type	Relative Orbit
Sentinel-1A	IW	Ascending	L1	SLC	45

Table 1: Characteristics of SAR images for the study area.

To obtain SLC products with the characteristics mentioned in the table above, from the script *download.py*, you must first fill in the configuration file, *download.conf*, with the appropriate parameters.

4.1.3 Interferometric Processing and Atmospheric Correction

To start processing the images, it is necessary to have SLC products and topographic delay maps available in the respective subdirectories.

The image of June 26, 2020 was chosen as the master, the configuration file (*project.conf*) was filled in with the respective paths and necessary parameters. After adjusting the configuration file, the interferometric process starts, using the previously mentioned scripts (figure 1).

As previously described, two Matlab scripts are generated which allow both the individual correction (*atm_correction.m*) and the chain correction (*main_auto_atm_correction.m*) of the interferograms.

In the figure 6, we can see five interferograms, before and after applying the correction, referring to the last interferograms of the processed time series:

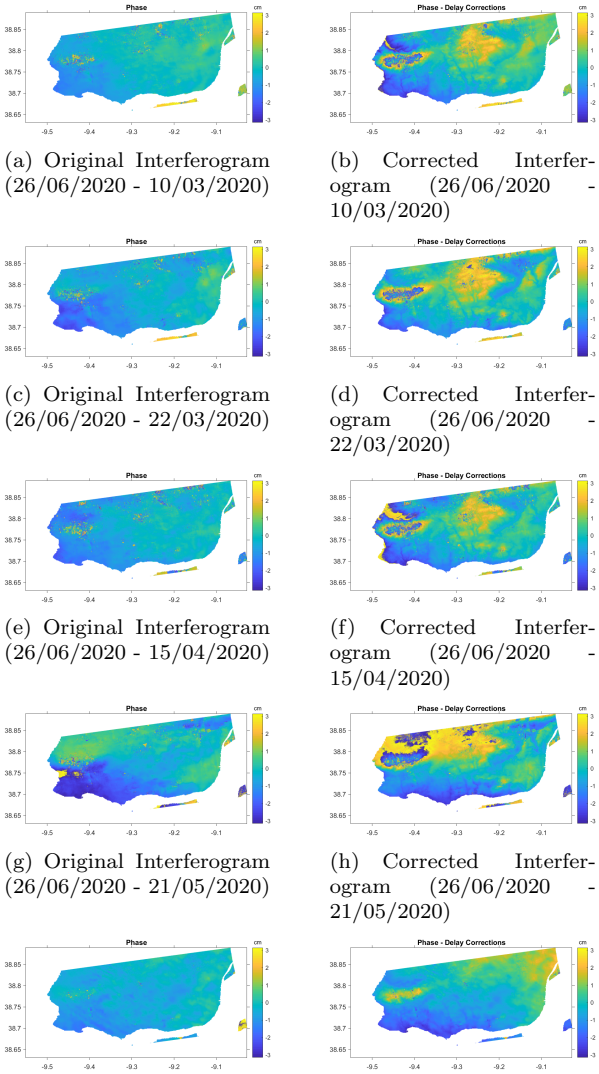

(a) Original Interferogram (26/06/2020 - 10/03/2020)

(b) Corrected Interferogram (26/06/2020 - 10/03/2020)

(c) Original Interferogram (26/06/2020 - 22/03/2020)

(d) Corrected Interferogram (26/06/2020 - 22/03/2020)

(e) Original Interferogram (26/06/2020 - 15/04/2020)

(f) Corrected Interferogram (26/06/2020 - 15/04/2020)

(g) Original Interferogram (26/06/2020 - 21/05/2020)

(h) Corrected Interferogram (26/06/2020 - 21/05/2020)

(i) Original Interferogram (26/06/2020 - 14/06/2020)

(j) Corrected Interferogram (26/06/2020 - 14/06/2020)

Figure 6: Interferograms before and after atmospheric correction for the last processed SAR products.

4.2. Comparison between corrected interferograms

From the file generated (*ifg_comparation.txt*) regarding the comparisons between the interferograms corrected sequentially, which means, between an interferogram in

process with the interferogram corrected in the previous instant, the data shown in figures 7 and 8 were obtained.

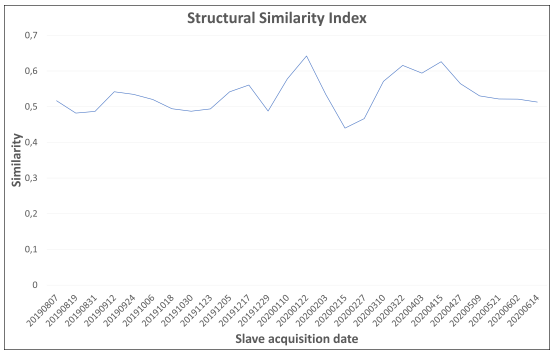

Figure 7: Structural similarity index between sequentially corrected interferograms.

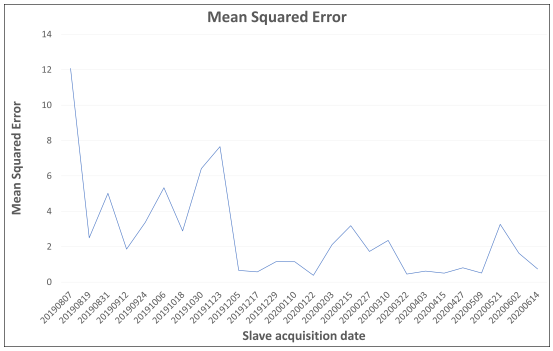

Figure 8: Mean squared error between sequentially corrected interferograms.

From the graph 7 related to the Structural Similarity Index, it can be seen that the values are mostly above 0.5, which reveals a high perceptual rate of similarity between the interferograms.

From the graph 8 relative to the mean quadratic error, it can be seen that there was a decrease in the error with the progress of the processing and a decrease in temporal baseline.

These values and variations can be partially justified with the long temporal baseline and the "short" perpendicular baseline of the products used, since one of the crucial steps for generating a subsidence map or a Digital Elevation Model (DEM) as well successful is the selection of the image pair with the appropriate properties. The time between the images must be as short as possible to reduce the risk of phase de-correlation of the phase and the distance between the positions of the satellites at the time of image acquisition must be between 150 and 300 meters [18].

4.3. Visualization of spatial data

To view the interferograms obtained after removing the effect from the atmosphere, a WebSIG was used, the *iMSEP* (internet-based information Management System for Environmental Protection and Disaster Risk Management), in order to allow the general public to view, analyze and share geographic information.

iMSEP (https://imsep.gis.lu.se/) was developed at Lund University, under the European project EMME of which IST-UL is a partner, under the coordination and management of Associate Professor Dr. Ali Mansourian.

In the figure 9 we can see some of the results obtained at the end of processing:

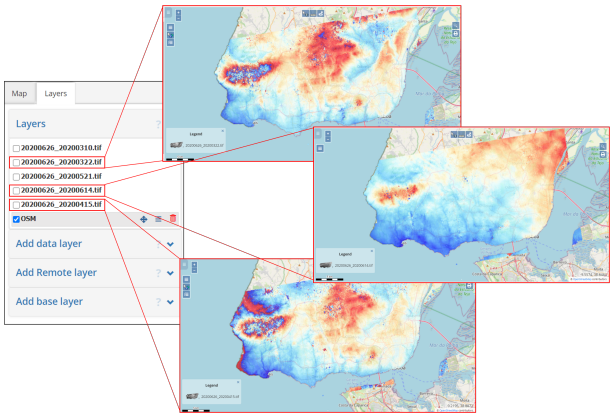

Figure 9: Partial visualization of the corrected interferograms on the iMSEP platform.

To view all the results obtained, consult the platform *iMSEP*, https://imsep.gis.lu.se/.

5. Conclusions

Earth observation data files are expanding at an unprecedented rate, both in terms of size and variety. More and more, existing and developing remote mapping sensors provide or will provide Earth observation data, characterized by large coverage, high spatial resolutions and high revisiting frequencies. In parallel, the power of computing is growing, thus allowing the processing of these data on a global scale, representing a unique opportunity in the study and the integrated knowledge of spatial phenomena on a scale of the entire Earth's surface.

This work started with the apresention of the basic aspects of SAR systems and some space missions that use these radars, with greater emphasis on the Copernicus - Sentinel-1 program. The concepts related to interferometry using SAR images were shown and the different stages that make up the interferometric process were briefly addressed. Equally worthy of attention are aspects related to spatial data infrastructures, which are interoperability infrastructures, due to the ability of different applications that use different languages or concepts to communicate with each other. The components related to the architecture of these systems were analyzed and two platforms (an InSAR platform and a Geoportal platform) were exemplified, with some of their more technical references.

Following the aforementioned, a versatile processing line was created, capable of processing SAR data, producing interferograms and removing the effect of the atmosphere during the phase using an online platform, to be later compared and visualized on an online platform. As a case study, interferograms referring to the period between July 2019 and June 2020 were created and corrected to approximately one calendar year, in the region covered by the municipalities of Lisbon, Oeiras

and Cascais. These results are available for consultation on the iMSEP spatial data visualization platform (https://imsep.gis.lu.se/), available under the European project EMME (*International MSc Educational Programme in Environmental Management and Modelling*).

In the production of the interferometric chain, the image of June 26, 2020 was considered as master and in total 27 interferograms were calculated and made available. For all, the atmospheric corrections provided by the GACOS platform were applied, which although satisfactory on a global scale, insofar as corrections related to the correlation of atmospheric effects with the terrain are observed, are not sufficiently detailed for a finer analysis. This is an expected fact, given that GACOS is a solution designed for studies of large areas (for example, for an entire interferometric range). In order to streamline the interpretation of results, a script was created that compares sequential interferograms pixel by pixel. In this assessment, variables related to structural similarity indices and mean square error were used.

6. Acknowledgments

The author would like to acknowledge Prof. Agostinho Rui Alves da Fonseca (Instituto Superior Técnico) and Prof. Ana Paula Martins Falcão Flôr (Instituto Superior Técnico).

References

[1] K. S. Andy Hooper, David Bekaert. *Sentinelsat Documentation*. Sentinelsat, 2019. URL `https://sentinelsat.readthedocs.io/_/downloads/en/stable/pdf/`.

[2] ASI. Cosmo-skymed, 2020. URL `https://www.asi.it/en/earth-science/cosmo-skymed/`. Acedido: 2020-09-05.

[3] R. Bamler. Principles of synthetic aperture radar. *Surveys in Geophysics*, 21(2-3):147–157, 2000.

[4] L. Bernard and M. Craglia. Sdi-from spatial data infrastructure to service driven infrastructure. In *Research Workshop on Cross-Learning Between Spatial Data Infrastructures and Information Infrastructures, Enschede, The Netherlands*. Citeseer, 2005.

[5] N. R. Budhathoki, Z. Nedovic-Budic, et al. Reconceptualizing the role of the user of spatial data infrastructure. *GeoJournal*, 72(3-4):149–160, 2008.

[6] Canada. What is radarsat-1, 2020. URL `https://www.asc-csa.gc.ca/eng/satellites/radarsat1/what-is-radarsat1.asp`. Acedido: 2020-09-05.

[7] C. W. Chen and H. A. Zebker. Network approaches to two-dimensional phase unwrapping: intractability and two new algorithms. *JOSA A*, 17(3):401–414, 2000.

[8] C. W. Chen and H. A. Zebker. Two-dimensional phase unwrapping with use of statistical models for cost functions in nonlinear optimization. *JOSA A*, 18(2):338–351, 2001.

[9] C. W. Chen and H. A. Zebker. Phase unwrapping for large sar interferograms: Statistical segmentation and generalized network models. *IEEE Transactions on Geoscience and Remote Sensing*, 40(8):1709–1719, 2002.

[10] C. Cipolloni. *Architecture of Spatial Data Infrastructure (SDI) (DRAFT)*, 2018.

[11] CLMS. European ground motion service: Service implementation plan and product specification document, 2020.

[12] N. R. Council, M. S. Committee, et al. *Toward a coordinated spatial data infrastructure for the nation*. National Academies Press, 1993.

[13] DLR. Terrasar-x - germany's radar eye in space, 2020. URL `https://www.dlr.de/content/en/articles/missions-projects/terrasar-x/terrasar-x-earth-observation-satellite.html`. Acedido: 2020-09-05.

[14] ESA. Sentinel-1 overview, September 2013. URL `https://sentinel.esa.int/web/sentinel/missions/sentinel-1/overview`. Acedido: 2020-08-22.

[15] ESA. Overview, 2017. URL `https://scihub.copernicus.eu/userguide/WebHome`. Acedido: 2020-08-22.

[16] ESA. Satellite frequency bands, 2019. URL `https://www.esa.int/Applications/Telecommunications_Integrated_Applications/Satellite_frequency_bands`. Acedido: 2020-08-09.

[17] ESA. Copernicus open access hub, batch scripting - dhusget script, 2020. URL `https://scihub.copernicus.eu/twiki/do/view/SciHubUserGuide/BatchScripting#dhusget_script`. Acedido: 2020-08-22.

[18] A. Ferretti, A. V. Monti-Guarnieri, C. Prati, F. Rocca, D. Massonnet, et al. *INSAR Principles B*. ESA publications, 2007.

[19] L. P. S. Fortes and V. O. H. de Araújo. Permanent committee for geospatial data infrastructure of the americas (pc-idea), 2013.

[20] GACOS. Gacos, 2017. URL `http://ceg-research.ncl.ac.uk/v2/gacos/`. Acedido: 2020-08-28.

[21] R. M. Goldstein and C. L. Werner. Radar interferogram filtering for geophysical applications. *Geophysical research letters*, 25(21):4035–4038, 1998.

[22] R. M. Goldstein, H. A. Zebker, and C. L. Werner. Satellite radar interferometry: Two-dimensional phase unwrapping. *Radio science*, 23(4):713–720, 1988.

[23] R. Hanssen. *Radar Interferometry: Data Interpretation and Error Analysis*. Remote Sensing and Digital Image Processing. Springer Netherlands, 2001. ISBN 9780792369455. URL `$https://books.google.pt/books?id=bqNkJUk4wtMC$`.

[24] A. Hooper. A multi-temporal insar method incorporating both persistent scatterer and small baseline approaches. *Geophysical Research Letters*, 35(16), 2008.

[25] Y. Huang and J. Van Genderen. Comparison of several multi-look processing procedures in insar processing for ers-1&2 tandem mode. In *ERS SAR Interferometry*, volume 406, page 215, 1997.

[26] JAXA. About alos-palsar, 2020. URL `https://www.eorc.jaxa.jp/ALOS/en/about/palsar.htm`. Acedido: 2020-09-05.

[27] M. Klopfer. Interoperability & open architectures: an analysis of existing standardisation processes & procedures. *OGC White Paper. Consortium, OG, Open Geospatial Consortium: 26p*, 2005.

[28] T. Lillesand, R. W. Kiefer, and J. Chipman. *Remote sensing and image interpretation*. John Wiley & Sons, 2004.

[29] D. J. Maguire and P. A. Longley. The emergence of geoportals and their role in spatial data infrastructures. *Computers, environment and urban systems*, 29(1):3–14, 2005.

[30] K. C. Marcel Wille. *StaMPS/MTI Manual.*, 2013.

[31] A. Moreira, P. Prats-Iraola, M. Younis, G. Krieger, I. Hajnsek, and K. P. Papathanassiou. A tutorial on synthetic aperture radar. *IEEE Geoscience and Remote Sensing Magazine*, 1(1):6–43, 2013.

[32] NG. The nationall geoportal, 2017. URL `http://www.pcn.minambiente.it/mattm/en/the-national-geoportal/`. Acedido: 2020-09-14.

[33] NGU. Insar norway, 2018. URL `https://www.ngu.no/en/topic/insar-norway`. Acedido: 2020-09-14.

[34] A. Phillips, I. Williamson, and C. Ezigbalike. Spatial data infrastructure concepts. *Australian Surveyor*, 44(1):20–28, 1999.

[35] A. Rajabifard and I. P. Williamson. Spatial data infrastructures: concept, sdi hierarchy and future directions. 2001.

[36] A. Rajabifard, F. Escobar, and I. P. Williamson. Hierarchical spatial reasoning applied to spatial data infrastructures. *Cartography*, 29(2):41–50, 2000.

[37] F. Rocca. An overview of sar interferometry. In *Proc. 3re ERS Symp, Florence, 1997*, 1997.

[38] R. Rossi. Considerazioni sui nuovi servizi di conversione di coordinate del geoportale nazionale. *GEOmedia*, 16(6), 2012.

[39] M. G. Tait. Implementing geoportals: applications of distributed gis. *Computers, Environment and Urban Systems*, 29(1):33–47, 2005.

[40] I. H. Woodhouse. *Introduction to microwave remote sensing*. CRC press, 2005.

[41] C. Yu, N. T. Penna, and Z. Li. Generation of real-time mode high-resolution water vapor fields from gps observations. *Journal of Geophysical Research: Atmospheres*, 122(3): 2008–2025, 2017. doi: 10.1002/2016JD025753.

[42] C. Yu, Z. Li, and N. T. Penna. Interferometric synthetic aperture radar atmospheric correction using a gps-based iterative tropospheric decomposition model. *Remote Sensing of Environment*, 204:109 – 121, 2018. ISSN 0034-4257. doi: https://doi.org/10.1016/j.rse.2017.10.038.

[43] C. Yu, Z. Li, N. T. Penna, and P. Crippa. Generic atmospheric correction model for interferometric synthetic aperture radar observations. *Journal of Geophysical Research: Solid Earth*, 123(10):9202–9222, 2018.

[44] H. A. Zebker and Y. Lu. Phase unwrapping algorithms for radar interferometry: residue-cut, least-squares, and synthesis algorithms. *JOSA A*, 15(3):586–598, 1998.

[45] H. A. Zebker, P. A. Rosen, R. M. Goldstein, A. Gabriel, and C. L. Werner. On the derivation of coseismic displacement fields using differential radar interferometry: The landers earthquake. *Journal of Geophysical Research: Solid Earth*, 99(B10):19617–19634, 1994.

[46] Zhou Wang, A. C. Bovik, H. R. Sheikh, and E. P. Simoncelli. Image quality assessment: from error visibility to structural similarity. *IEEE Transactions on Image Processing*, 13(4):600–612, 2004. doi: 10.1109/TIP.2003.819861.